Crack Path and Fracture Toughness Predictions for Welded Aluminium Sheets

D. Steglich, P. Nègre, W. Brocks

GKSS Research Center Geesthacht, Germany

ABSTRACT. *The ductile fracture behaviour of an undermatched aluminium weld is investigated experimentally and simulated numerically by two different models of ductile damage, namely the microstructure-based Gurson-Tvergaard-Needleman model and a phenomenological cohesive model. The model parameters for the different material zones are determined by a hybrid approach combining microstructural analyses, mechanical testing and numerical simulations. Particular emphasis is placed on a configuration where the initial crack is located in the heat affected zone and extends into the softer fusion zone. A simplified model of a bi-material system with a crack at the interface is used to simulate crack path deviation.*

INTRODUCTION

About 60 % of a modern passenger aircraft are made of aluminium. Improved welding techniques have been developed to save productions costs and weight while guaranteeing performance and safety at the same time. Damage tolerance is required for aircraft structures, which means that defects such as small fatigue cracks extending during service do not interfere with its integrity. This is why the residual strength of cracked components has to be realistically predicted. Whereas initiation of crack extension under quasistatic loading is the critical scenario for determining maximum load in thick-walled components, stable crack extension may occur in thin-walled structures, before maximum load is reached.

Conventionally, ductile crack extension under quasi-static loading is characterised by an R-curve, which is some appropriate "driving force" such as the *J*-integral or CTOD (crack tip opening displacement) in dependence on crack extension, Δa. Application of the J-integral requires a homogeneous material and a number of geometrical conditions for the specimens, from which R-curves are determined. Neither of these requirements is met for welded sheet metal. Enhanced concepts for strength-mismatched configurations [1] and thin-walled structures [2] have been proposed, particularly based on CTOD. Additional problems arise, however, for the determination of "valid" R-curves in undermatched welded joints, if the initial crack is not positioned exactly in the fusion zone and may deviate from its original plane after initiation. All of this gives rise

to approach the problem with more advanced models based on local damage evolution, which are not restricted with respect to the geometry.

The resistance of the material to damage can be analysed by experiments and numerical simulations. Experimental determination of the fracture resistance is generally carried out on laboratory coupons whose geometry and loading conditions try to represent the service conditions of a component or a structure. Due to the high cost of such tests only a limited amount of full scale structure tests exist. Nowadays, the use of computational mechanics permits to simulate the behaviour of complex structures with high accuracy. The combined use of experimental investigations and numerical simulations (hybrid methods) permits the validation of damage models and allows for an improved understanding of the failure mechanisms.

Material properties and microstructures in a welded joint vary in dependence on the distance to the fusion line, and three major zones are commonly distinguished: The base metal (BM), the heat affected zone (HAZ) and the narrow fusion zone (FZ). Whereas BM and FZ have different but comparatively homogeneous properties, the HAZ is inhomogeneous with respect to both microstructure and mechanical properties. Aluminium welds are typically undermatched, i.e. the strength of the weld metal is lower than that of the base material, which is characterised by the mismatch factor M as the ratio between the yield strengths of FZ and BM, which is 0.67 in the present case.

Ductile crack growth in aluminium alloys occurs by the formation and growth of micro-cavities, which form at dispersoids and second phase particles. Two different models are applied in this contribution: the Gurson-Tvergaard-Needleman model and the cohesive model. These two models present different approaches to simulate crack extension. The first one, the GTN-model, is based on the idea that fracture results from the process of void nucleation, growth and coalescence whereas the cohesive model considers the evolution of the crack through the separation of the two crack surfaces in the process zone. Another difference between the two models resides in their implementation in a FE-code. The GTN-model is a coupled model and the continuum elements behave accordingly to the GTN plastic potential that accounts for damage evolution, whereas the cohesive elements are interface elements that are placed between the continuum elements following the von Mises plasticity. These two models are applied to simulate crack extension of the aluminium laser weld under static loading. The model parameters for the different material zones are determined by a hybrid approach combining microstructural analyses, mechanical testing and numerical simulations. Special emphasis is put on the prediction of the proper crack extension direction, as both models are generally able to predict the crack path from local field variables.

CHARACTERISATION OF Al6056 T78

Microstructures

The microstructure of the laser weld is investigated using polished specimens under optical microscope (OM) and scanning electron microscope (SEM). The base material´s

microstructure is typical of that of 6xxx series aluminium alloys. It possesses two populations of coarse particles and a population of dispersoids. The grains in the BM are elongated due to rolling of the casting to achieve the required thickness with an aspect ratio (length/width) equal to 4.

The microstructure of the weld metal (FZ) is not uniform. At the top middle of the FZ, equiaxed grains (called epitaxial grains) are visible whereas the remaining part of the FZ contains columnar grains. This type of microstructure in the weld with two populations of grains is typical of aluminium alloy welds. The heat affected zone possesses microstructural features of both regions (i.e FZ and BM). Close to the BM, the grains are elongated with an aspect ratio similar to the one of the BM whereas close to the FZ the grains become larger. The inclusion morphology is quantified by particle diameter and nearest neighbour distance (NND) distribution and given in Table 1.

Table 1. particle morphology

Material	V_p (%)	$d_{inclusions}$ (μm)		NND (μm)
		average	maximal	
Al6056 T78 BM	1.15	3.46	18	< 40
Al6056 T78 FZ	3.5	0.7	18	< 10

Mechanical Properties

Round tensile specimens as commonly used to determine uniaxial stress-strain curves of a material are unfit for sheet metal. In particular, the material gradients occurring in a welded joint require small-sized specimens, and characterisation of a narrow laser weld makes high demands on mechanical testing. Micro flat tensile specimens (MFT) with 0.5×2 mm^2 cross section have been used to measure local stress-strain curves. Representative tensile results in terms of engineering stress vs. strain curves are plotted in Figure 1. Variations of stresses and ductility are observed between the different regions of the laser weld. The fusion zone has the lowest yield strength ($\sigma_{0.2FZ}$=200 MPa) and fracture appears at low plastic strains. The ductility is around 2 %. Materials in the HAZ and BM show low strain hardening behaviour and a higher ductility. In both regions, the strain at rupture is around 10 %. High variation of yield strength and tensile strength is observed for the material in the HAZ, the scatter of these values is represented by the grey area in Figure 1. In the BM, the material appears to be homogeneous. The proof stress of the base material is $\sigma_{0.2BM}$=302 MPa.

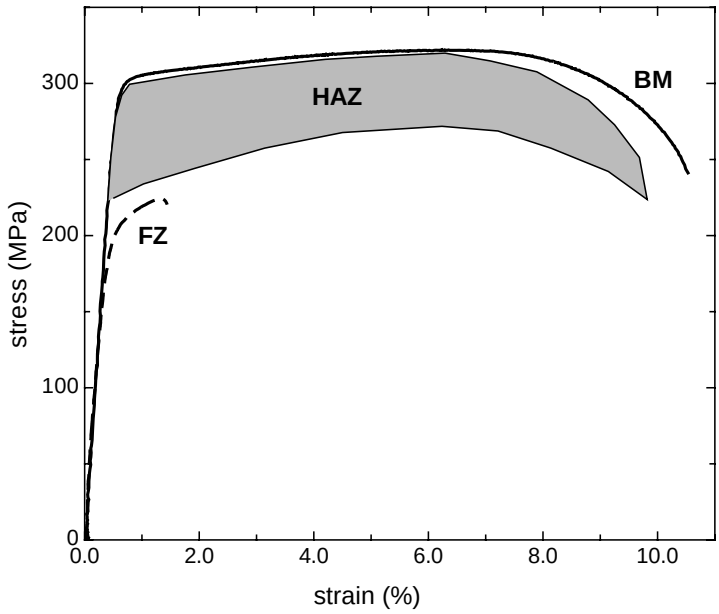

Figure 1. Yield curves of Al6056 T78 LBW

Fracture Toughness

Fracture resistance is characterised by CTOD, δ_5, vs. crack extension, Δa, see Schwalbe et al. [2]. Tests of laser beam welded Al6056 have been carried out using compact tension specimens (C(T)-specimen, W=50 mm, a/W=0.5, B=4.2 mm). A sketch of the specimen is provided in Figure 2. The specimens were statically loaded perpendicular to the rolling direction. The initial crack was introduced in the BM (Figure 2a), in the middle of the FZ (Figure 2b) and within the HAZ (Figure 2c). Due to the undermatch configuration, for configuration (b) the crack extends in the FZ.

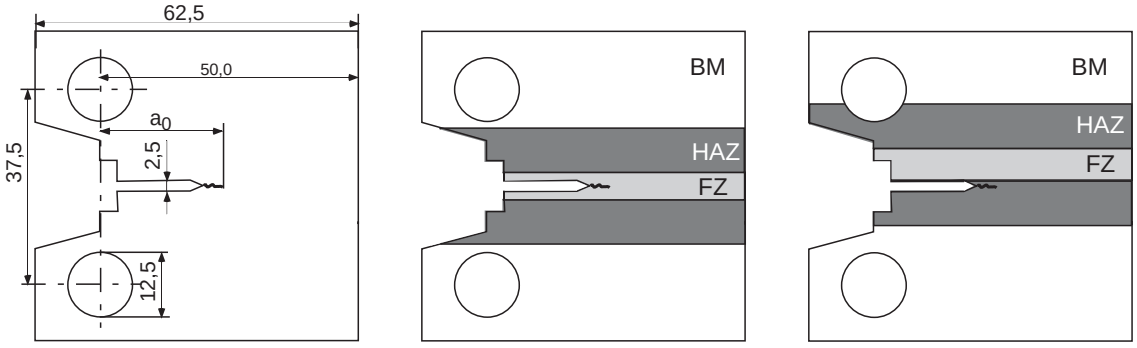

a) initial crack in BM b) initial crack in the middle of the FZ c) initial crack in the HAZ

Figure 2. Initial crack configurations investigated, measures in mm

Investigations of fractured specimens have shown that a crack initially located in the HAZ (corresponds to Figure 2c) deviates towards the FZ, which has a significant lower toughness. The topography of the fracture surface of two fractured specimens is presented in Figure 3, exhibiting an average inclination angle of 17°. Crack path deviations from the ligament between 10° and 25° have been measured on different specimens. This raises the question how to determine valid toughness data.

Though the measured fracture toughness of a weld is affected not only by the weld material but also by the weld geometry, particularly its width to length ratio, it is taken as a valid value as long as the crack remains in the same material zone. Thus, configuration (b) would yield a "valid" fracture toughness, but configuration (c) would not due to crack path deviation. The respective effect will be investigated by means of numerical simulations with damage models.

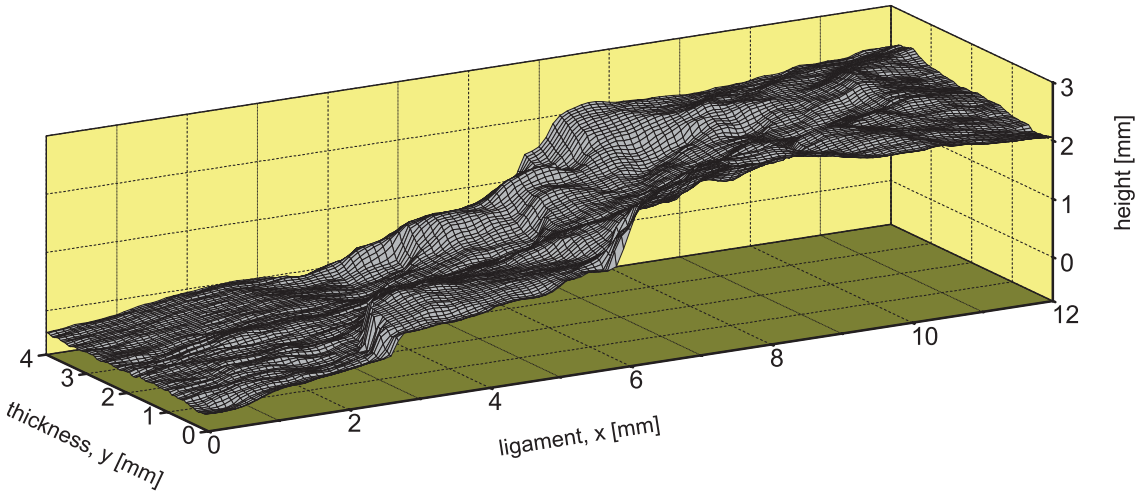

Figure 3. Topography of a fracture surface for an initial crack in the HAZ

MODELLING APPROACHES

Damage models can be used to describe the micromechanical mechanisms of void nucleation, growth and coalescence in the framework of continuum mechanics. Damage parameters are commonly related to microstructural properties of the respective material. The mesoscopic yield condition for a porous plastic solid as used in this study was first derived by Gurson [3] by analysing a spherical void in an infinite rigid – perfectly plastic medium (matrix). The original yield condition was later modified by Tvergaard and Needleman [4,5] and reads:

$$\Phi = \frac{\sigma_{\mathrm{eq}}^2}{R^2(\varepsilon_p)} + 2q_1 f^* \cosh\left(\frac{q_2}{2}\frac{\sigma_{kk}}{R(\varepsilon_p)}\right) - 1 - q_3 f^{*2} = 0 \qquad (1)$$

$$f^* = \begin{cases} f & \text{for } f \le f_c \\ f_c + K(f - f_c) & \text{for } f > f_c \text{ with } K = \dfrac{f_u^* - f_c}{f_f - f_c} \end{cases} . \qquad (2)$$

This relation accounts for isotropic strain hardening by taking the flow stress, R, of the matrix material surrounding the void to be dependent on the accumulated equivalent plastic strain, ε_p. Damage is described by the internal variable f^*, which is a function of the void volume fraction f (ratio of the total volume of all cavities to the volume of the body). Void interaction effects starting at a critical void volume fraction, f_c, are accounted for by the use of the damage variable, f^*, in the yield function. Accelerated damage evolution is then defined by the scalar constant K.

The cohesive model is a phenomenological model based on the strip yield models of Dugdale [6] and Barenblatt [7]. The material's behaviour is split into two parts: deformation and separation. In the framework of finite elements, deformation is accounted for by continuum elements representing an elastic–plastic material behaviour, whereas separation is modelled by interface elements, the cohesive elements. The separation of the cohesive elements is governed by a stress–displacement relationship, the so-called traction–separation law (TSL). The model parameters for a given TSL are the maximum stress of the cohesive elements, T_0, and a critical separation at which the stress carrying capacity of the cohesive elements vanishes, δ_0. From both quantities, the cohesive energy Γ_0 can be calculated. The cohesive law used in the present investigations is written as:

$$T(\delta) = T_0 \begin{cases} 2\left(\frac{\delta}{\delta_1}\right) - \left(\frac{\delta}{\delta_1}\right)^2 & \delta < \delta_1 \\ 1 & \delta_1 < \delta < \delta_2 \\ 2\left(\frac{\delta-\delta_2}{\delta_0-\delta_2}\right)^3 - 3\left(\frac{\delta-\delta_2}{\delta_0-\delta_2}\right)^2 + 1 & \delta_2 < \delta < \delta_0 \end{cases} \qquad (3)$$

With δ_1 and δ_2 as parameters defining the function´s shape.

SIMULATION OF CRACK EXTENSION

Parameter Identification

The model parameters for the different material zones have been determined by a hybrid approach combining microstructural analyses, mechanical testing and numerical simulations, see Nègre et al. [8,9]. The yield curves are obtained from simulations of tensile tests of MFT specimens (Figure 1). The GTN damage parameters are partly identified from microstructural analyses and partly from simulations of the fracture tests on the C(T) specimens (a) and (b), and so were the cohesive parameters. As the crack in configuration (b) extends in the FZ, the GTN as well as the cohesive parameters characterise the weld material. Figure 4 shows the simulated resistance curves of both

models compared to the test results for both configurations, initial crack in BM (a) and in FZ (b). The model parameters identified are given in Table 2. They are now applied to a crack at the interface between HAZ and FZ.

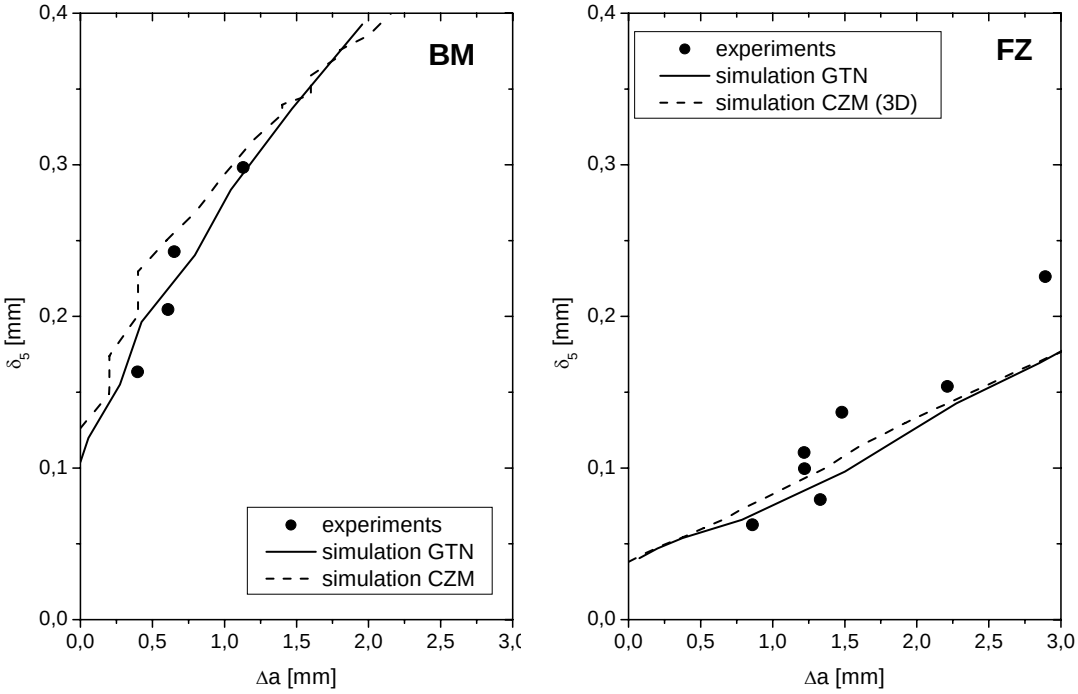

Figure 4. Fracture resistance curves: experiment and simulations - corresponding to configurations (a) and (b)

Crack Path Deviation of HAZ Crack

A full representation of the various material zones and their particular properties in an FE model would exceed any reasonable effort, the more so as the transition between these zones is blurred and the exact determination of the actual crack locations in the test specimens is practically impossible. For simplicity, the problem is treated as a bi-material configuration with an interface crack. The tensile properties of the HAZ adjacent to the FZ were found to be identical to the BM. All the other gradients of material properties are not taken into account.

In addition to the choice of appropriate constitutive models and calibration of their parameters, the selection of a proper structural model is essential. Generally, both the GTN and the cohesive model are applicable in 2D and 3D simulations. The global mechanical response of thin panels is well represented by plane stress models. The stress state at the crack tip is close to plane strain, however, and hence local models of crack extension may fail or yield wrong predictions under plane-stress conditions. This

is particularly vital for models of porous plasticity, where void growth depends on the hydrostatic stress. Pure plane-stress models will severely underestimate crack extension or show non at all. Hence, a full 3D structural model has been chosen for the GTN model in the present study. The element height has to be related to the average spacing of void nucleating particles via the separation energy [10,11]. As deviation of the crack from its originally straight path is expected, the elements in the ligament should be chosen vertically elongated [12,8]. The element dimensions have been fixed as $70 \times 150 \times 210\ \mu m^3$ for the FZ and $200 \times 150 \times 210\ \mu m^3$ for the BM.

Table 2. GTN and CZM parameters

	R_0 [MPa]	n	f_0	f_c	K	q_1	q_2	Γ_0 [N/mm]	T_0 [MPa]
FZ	200	0.25	0.035	0.16	3	1.5	1.1	8	440
BM	302	0.67	0.0115	0.0195	5	1.5	1.0	30	570

The phenomenological cohesive model suggests a less costly 2D simulation. As stated above already, plane-stress elements cannot correctly reproduce the triaxiality at the crack tip, which may have detrimental effects on the cohesive model, too. As $\sigma_{33}=0$, the maximum principal stress, σ_{22}, is limited by the actual flow stress, $R(\varepsilon_P)$, and since the cohesive strength, T_0, is typically larger than $R(\varepsilon_P)$, this leads to strain localisation within the solid elements in the process zone inhibiting further crack extension. One way of circumventing this problem is the introduction of a plane-strain core along the ligament [13]. Strain localisation in the plane-stress elements can also be prevented by accounting for the thickness reduction of the solid elements and transferring this information to the cohesive elements [14]. This does not correct the underestimation of stress triaxiality at the crack tip, of course. In the present investigations, a plane-strain core has been introduced for several reasons: (i) the assignment of cohesive elements to neighbouring solid elements, which is required for transferring the information of thickness reduction, is tricky, if crack path kinking is admitted; (ii) the strength mismatch causes an additional increase of triaxiality in the FZ; (iii) a realistic estimate of the width of the plane-strain core could be derived from the GTN simulations. Figure 5 shows the deviated crack obtained from GTN (left) and CZ (right) simulations.

CONCLUSIONS

The resistance to stable crack extension of the aluminium alloy 6056 and its weld has been investigated by means of fracture mechanics tests using homogeneous base material and welded specimens. In the last case, the initial crack is either within the fusion zone or in the heat affected zone. Due to the mismatch in mechanical properties, the crack starting in the HAZ deviates from its original path (normal to the loading direction) towards the fusion zone. The crack deflection has been quantified through

topography measurements of the fracture surface. The crack deviation angle varies between 10° and 25° with an average value of 17°.

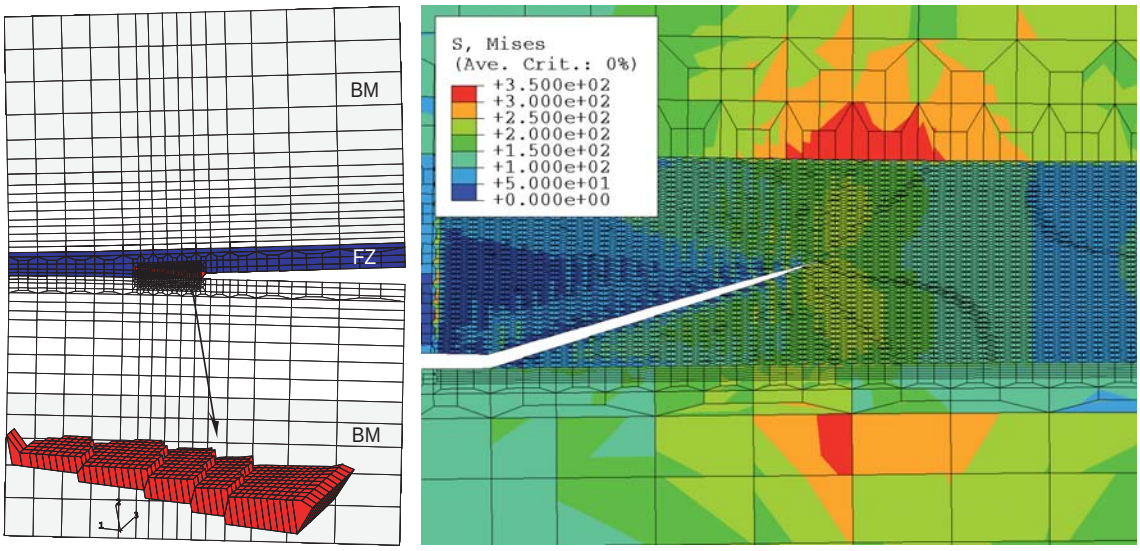

Figure 5. Crack path predictions with the GTN-model (left) and CZM (right)

Crack extension analyses of configurations with initial crack in the base material and the fusion zone yield the parameters of local damage models models for the respective zones. Using these parameters, crack path predictions can be made for asymmetric configurations (crack in the heat affected zone). In particular, the following statements can be derived:

- Using the Gurson-Tvergaard-Needleman model, a relationship between the microscopic scale and the macroscopic properties of the material and its weld can be established.
- Since no standardised methods exist up to now to characterise the resistance to stable crack extension of a weld, the cohesive model is an attractive tool, particularly for engineers. The physically based model is relatively "easy" to handle and can also be employed to quantify the fracture toughness of components.
- Porosity models combined with the use of 3D finite elements are capable to simulate crack extension in low triaxiality sheet metal.
- The deviation of the crack path can be numerically predicted. The crack trajectory affects only slightly the fracture behaviour of the weld.

REFERENCES

1. Schwalbe, K.H., Kim, Y.-J., Hao, S., Cornec, A., and Koçak, M.: EFAM ETM-MM 96 (1997).
2. Schwalbe, K.H., Newman, J.C., and Shannon, J.L. Engng. Fract. Mech. 72 (2005), 557-576.
3. Gurson, A.L., J. Eng. Mater. Technol.-Trans. ASME, 99 (1977) 2-15.
4. Needleman, A. and Tvergaard, V., J. Mech. Phys. Solids, 32 (1984) 461-490.
5. Needleman, A. and Tvergaard, V., J. Mech. Phys. Solids, 35 (1987) 151-183.
6. Dugdale, D.S., J. Mech. Phys. Solids, 8 (1960) 100-104.
7. Barenblatt, G., Advances in Applied Mechanics, 7 (1962) 55-129.
8. Nègre, P., Steglich, D., and Brocks, W., Eng. Fract. Mech., 71 (2004) 2365-2383.
9. Nègre, P., Steglich, D., and Brocks, W., Int. J. Fracture, 134 (2005) 209-229.
10. Ruggieri, C., Panontin, T.L., and Dodds, R.H. (1996) Int. J. Fracture 82, 67-95
11. Siegmund, T., and Brocks, W. (1999) Int. J. Fracture 99, 97-116.
12. Ostby, E. Dissertation. Trondheim, Norway, teknisk-naturvitenskapelige universitet.
13. Newman, J.C., Booth, B.C., and Shivakumar, K.N. (1988) In: Fracture Mechanics, 18th Symp., ASTM STP 945, 665-685.
14. Scheider, I., and Brocks, W. (2004) In: Thin-Walled Structures - Advances in Research, Design and Manufacturing, 483-490